Bone 106 (2018) 69–77

Contents lists available at ScienceDirect

Bone

journal homepage: www.elsevier.com/locate/bone

Full Length Article

Validation of calcaneus trabecular microstructure measurements by HR-pQCT

Louis M. Metcalf [a], Enrico Dall'Ara [b], Margaret A. Paggiosi [c], John R. Rochester [d], Nicolas Vilayphiou [e], Graham J. Kemp [f], Eugene V. McCloskey [a,b,*]

[a] MRC-Arthritis UK Centre for Integrated research into Musculoskeletal Ageing (CIMA), Department of Oncology and Metabolism, University of Sheffield, Metabolic Bone Centre, Northern General Hospital, Herries Road, Sheffield S5 7AU, UK
[b] Department of Oncology and Metabolism and INSIGNEO Institute for in silico Medicine, University of Sheffield, The Pam Liversidge Building, Sir Robert Hadfield Building, Mappin Street, Sheffield S1 3JD, UK
[c] The Mellanby Centre for Bone Research, Department of Oncology and Metabolism, University of Sheffield, Metabolic Bone Centre, Northern General Hospital, Herries Road, Sheffield S5 7AU, UK
[d] Academic Unit of Medical Education, Medical School, University of Sheffield, Medical Education, The Medical School, Beech Hill Road, Sheffield S10 2RX, UK
[e] SCANCO Medical AG, Fabrikweg 2, 8306 Brüttisellen, Switzerland
[f] MRC-Arthritis UK Centre for Integrated research into Musculoskeletal Ageing (CIMA), Institute of Ageing and Chronic Disease, University of Liverpool, Liverpool, Department of Musculoskeletal Biology, William Henry Duncan Building, West Derby Street, Liverpool L7 8TX, UK

ARTICLE INFO

Article history:
Received 21 April 2017
Revised 22 August 2017
Accepted 20 September 2017
Available online 3 October 2017

Keywords:
Calcaneus
Trabecular microstructure
High-resolution peripheral quantitative computed tomography
Micro computed tomography

ABSTRACT

Objective: Assessment of calcaneus microstructure using high-resolution peripheral quantitative computed tomography (HR-pQCT) might be used to improve fracture risk predictions or to assess responses to pharmacological and physical interventions. To develop a standard clinical protocol for the calcaneus, we validated calcaneus trabecular microstructure measured by HR-pQCT against 'gold-standard' micro-CT measurements.
Methods: Ten human cadaveric feet were scanned *in situ* using HR-pQCT (isotropic 82 μm voxel size) at 100, 150 and 200 ms integration times, and at 100 ms integration time following removal of the calcaneus from the foot (*ex vivo*). Dissected portions of these bones were scanned using micro-computed tomography (micro-CT) at an isotropic 17.4 μm voxel size. HR-pQCT images were rigidly registered to those obtained with micro-CT and divided into multiple 5 mm sided cubes to evaluate and compare morphometric parameters between the modalities. Standard HR-pQCT measurements (derived bone volume fraction (BV/TV^d); trabecular number, Tb.N; derived trabecular thickness, $Tb.Th^d$; derived trabecular spacing, $Tb.Sp^d$) and corresponding micro-CT voxel-based measurements (BV/TV, Tb.N, Tb.Th, Tb.Sp) were compared.
Results: A total of 108 regions of interest were analysed across the 10 specimens. At all integration times HR-pQCT BV/TV^d was strongly correlated with micro-CT BV/TV ($r^2 = 0.95–0.98$, RMSE = 1%), but BV/TV^d was systematically lower than that measured by micro-CT (mean bias = 5%). In contrast, HR-pQCT systematically overestimated Tb.N at all integration times; of the *in situ* scans, 200 ms yielded the lowest mean bias and the strongest correlation with micro-CT ($r^2 = 0.61$, RMSE = 0.15 mm^{-1}). Regional analysis revealed greater accuracy for Tb.N in the superior regions of the calcaneus at all integration times *in situ* (mean bias = 0.44–0.85 mm^{-1}; $r^2 = 0.70–0.88$, $p < 0.001$ *versus* mean bias = 0.63–1.46 mm^{-1}; $r^2 \le 0.08$, $p \ge 0.21$ for inferior regions). $Tb.Sp^d$ was underestimated by HR-pQCT compared to micro-CT, but showed similar trends with integration time and the region evaluated as Tb.N. HR-pQCT $Tb.Th^d$ was also underestimated and moderately correlated ($r^2 = 0.53–0.59$) with micro-CT Tb.Th, independently from the integration time. Stronger correlations, smaller biases and error were found in the scans of the calcaneus *ex vivo* compared to *in situ*.
Conclusion: Calcaneus trabecular BV/TV^d and trabecular microstructure, particularly in the superior region of the calcaneus, can be assessed by HR-pQCT. The highest integration time examined, 200 ms, compared best with micro-CT. Weaker correlations for microstructure at inferior regions, and also with lower integration times, might limit the use of the proposed protocol, which warrants further investigation *in vivo*.

1. Introduction

Osteoporosis is characterized by a deterioration of bone mass and microstructure, resulting in loss of bone strength and increased risk of fracture [1]. Dual-energy X-ray absorptiometry (DXA) areal bone

* Corresponding author at: MRC-Arthritis UK Centre for Integrated research into Musculoskeletal Ageing (CIMA), Department of Oncology and Metabolism, University of Sheffield, Metabolic Bone Centre, Northern General Hospital, Herries Road, Sheffield S5 7AU, UK.
E-mail address: e.v.mccloskey@sheffield.ac.uk (E.V. McCloskey).

https://doi.org/10.1016/j.bone.2017.09.013

mineral density (BMD) is used as part of the routine assessment of osteoporosis, either alone or increasingly combined with an evaluation of risk factors independent of BMD as in tools such as FRAX [2]. The two-dimensional representation of bone properties captured by DXA measurements limits the technique's sensitivity to changes in bone microstructure with disease and with treatments for osteoporosis management. Clinical research studies have recently benefitted from being able to study bone microstructure using a significantly lower ionizing radiation dose and higher spatial resolution compared to standard quantitative computed tomography (QCT) at the spine and hip [3]. Such High-Resolution peripheral QCT (HR-pQCT) can identify trabecular and cortical microstructural abnormalities and mechanical deficiencies associated with fracture risk [4–6], and appear sensitive to changes induced by some treatments for osteoporosis [7–9].

The HR-pQCT scan has been performed primarily at the distal radius and distal tibia. Other sites have been scanned using HR-pQCT, such as the metacarpal joints [10,11] and there have been new developmental investigations at the knee [12]; these highlight quantitative outcomes that could be useful in areas other than osteoporosis research. The calcaneus (heel bone) has been widely investigated in osteoporosis, particularly using the attenuation of ultrasonic waves from quantitative ultrasound (QUS). The latter appears to provide microstructural information independent of BMD [13,14] and can predict vertebral and non-vertebral fracture risk [15]. However, there have been validity issues using QUS, specifically associated with its precision over time [16] and inter-device differences [17]. DXA scanning could be used in the calcaneus, however this would still suffer from the inherent limitations of areal measurements. In podiatry research, clinical computed tomography (CT) has been used to model the calcaneus and surrounding bones of the foot [18,19] and to clinically examine calcaneal fractures. In the assessment of calcaneus microstructure, measurements from multi-detector CT scans, with an in-plane pixel size of 208 μm and 500 μm slice thickness, have been weakly correlated ($r^2 \leq 0.51$) to measurements from micro-CT scans (16 μm voxel size) [20]. The use of HR-pQCT scans with a voxel size of 61 to 82 μm may improve the quantification of calcaneus microstructure *in vivo* and could therefore be of interest to the osteoporosis and podiatry fields; to our knowledge a method to scan the calcaneus using HR-pQCT has not been reported *in vivo*.

Distal radius and tibia trabecular and cortical microstructural and biomechanical HR-pQCT measurements have been validated in comparison to scans obtained using micro-CT [21–25]. Compared to the radius and tibia, the calcaneus is anatomically and structurally different; it is the largest tarsal bone and has several close-lying bones of the foot (talus, navicular and cuboid). Additionally, it is characterized by a thin cortex containing trabecular bone. We therefore aimed to develop a protocol to scan the calcaneus using HR-pQCT and validate measurements of trabecular microstructure. Specifically, we wanted to determine the accuracy of trabecular BV/TV and microstructure in calcaneus HR-pQCT scans with respect to 'gold standard' micro-CT measurements, and to explore the impact of scan integration time (*i.e.* the duration of each tomographic projection) on structural parameters.

2. Methods

2.1. Materials

Ten lower limbs were obtained from cadavers ($n = 5$, all female, age range 85 to 101 years) that had consented in life and were donated to the University of Sheffield for anatomical study. The cadavers had undergone standard embalming, which has been reported to have a minimal effect on BMD [26], and the limbs were divided through the proximal 2/3 point of the tibia. The use of the limbs was carried out under direct supervision of the Designated Individual, authorised under the Human Tissue Act and the limbs were returned after use. No medical history was available and specimens were not examined for the presence of metabolic bone disease. Ethical approval was provided by the Medical School Research Ethics Committee at the University of Sheffield (reference number 007375).

2.2. HR-pQCT scanning

The embalmed specimens were kept in sealed polythene bags during HR-pQCT scanning. Specimens were positioned in the carbon fiber foot cast that is normally used for the distal tibia HR-pQCT scan. The feet were positioned so that the superior and inferior surfaces of the calcaneus were parallel to the reference line that was positioned to start the scan: this enabled a series of lateral slices of the calcaneus to be obtained. *In vivo*, this would require a body and lower-limb position equivalent to the distal tibia HR-pQCT scan, but with plantar-flexion at the ankle. Scans of the whole calcaneus were obtained between the superior peak of the tuberosity and the plantar fascia attachment to the calcaneal tuberosity at an isotropic voxel size of 82 μm (maximum of 660 slices) using the standard clinical operational settings: 60 kVp and 95 mA collecting 750 projections over a 180° rotation of the X-ray source (XtremeCT I, SCANCO Medical AG; Brüttisellen, Switzerland). As part of the method development, each calcaneus was scanned with different integration times; *in situ* (with the calcaneus in the intact limb) scan projections were collected twice at 100 ms and once each at 150 and 200 ms integration times, labelled IS100, IS150 and IS200, respectively. The range of integration times was tested to determine the potential gains in microstructure assessment of more prolonged exposure, while limiting the upper scan time to 4.2 min to minimize potential movement artifacts when the protocol would be used *in vivo* in future clinical settings. Isolated *(ex-vivo*, with the calcaneus removed from the limb, soft tissue removed but no cleaning of the bone marrow) scan projections were collected at 100 ms integration time, labelled EV100, to determine whether measurements would be affected by the surrounding bones of the foot. For these scans, the calcaneal samples were placed in sealed polythene bags and supported by foam, in order to obtain a similar anatomical position to scans *in situ*.

Image reconstruction followed the manufacturer's standard methods. The reconstructed linear attenuation was mapped onto a 1536×1536 matrix and converted to hydroxyapatite (HA) densities. Calibrations of the densities were performed on a daily basis using a phantom supplied by the manufacturer, which has HA rods at 0, 100, 200, 400 and 800 mg HA/cm^{-3} embedded in resin.

2.3. Micro-CT scanning

The dissected calcanei were cut into rectangular prism samples ($18 \times 18 \times 40$ mm) preserving cortical bone at the superior and inferior surfaces, using a diamond-coated bandsaw under constant water irrigation (EXAKT, GmbH; Norderstedt, Germany). Each sample was submerged and fixed in a 50 ml holder containing saline solution and was vacuumed for 20 min to remove air bubbles prior to each scan.

Each sample was scanned at an isotropic voxel size of 17.4 μm using a SkyScan 1172 desktop micro-CT system (Brüker; Kontich, Belgium). Settings for image acquisition were 100 kVp, 100 μA, 2950 ms integration time, 2 frames averaged, 1.0 mm aluminum filter and a 0.7° rotation step. Scans were reconstructed using the NRECON software, according to the manufacturer's recommendations: ring artifact was set to 10, beam hardening to 30%, 16-bit DICOMs as applied in a recent study of human trabecular bone [27].

2.4. Rigid image registration

HR-pQCT scan DICOMs were registered to their respective micro-CT scans in a two-step process (Amira 6.0, FEI; Oregon, USA): step 1, an IS100 HR-pQCT scan was pre-aligned and registered to the micro-CT scan using a normalized mutual information metric and resampled using a Lanczos interpolator. The Lanczos interpolator has been applied to transform micro-CT scans of small animals [28,29]. A preliminary

study showed minimal effects of Lanczos interpolation when applied to HR-pQCT scans (Supplemental material 1). In step 2, the remaining HR-pQCT scans (IS100, IS150, IS200 and EV100) were registered using similar settings to the pre-registered IS100 HR-pQCT scan. This spatially registered all HR-pQCT scans to the micro-CT scan and, importantly, to the same reference system. The HR-pQCT scans from step 2 were used for morphological evaluation.

2.5. HR-pQCT and micro-CT evaluation

A custom cropping procedure was performed at the common region between the scan modalities, along the superior-inferior axis. The aim of the procedure was to increase the likelihood of evaluating a wider range of BV/TV [25,30] as there had been significant bone loss in some specimens. Images were divided into regions of interest approximately 5 × 5 × 5 mm in dimensions: HR-pQCT, 60 × 60 × 60 voxels and micro-CT 284 × 284 × 284 voxels (Fig. 1). 24 cubical regions of trabecular bone were isolated in each scan, virtually dividing the central portion of each micro-CT image in six 5 mm thick slices, which were divided into four cubes (Fig. 1). All registered HR-pQCT scans and the micro-CT scans were then imported into an XtremeCT workstation and evaluated using the SCANCO Image Processing Language (IPL 5.08-B).

HR-pQCT scans were evaluated using the standard patient analysis; this uses a Laplace-Hamming filter to smooth the image and enhance edges, and then applies a 40% fixed global threshold to segment the bone from marrow phase [31]. The following measurements were extracted from the images: trabecular volumetric BMD (Tb.vBMD), derived trabecular BV/TV (BV/TV^d; Tb.vBMD/1200), trabecular number (Tb.N) using ridge extraction methods [32] and derived trabecular thickness ($Tb.Th^d$; BV/TV^d/Tb.N) and spacing ($Tb.Sp^d$; (1-BV/TV^d)/Tb.N) using plate-model assumptions [33,34].

Micro-CT scans underwent a Gaussian filter (kernel 1.2, support 2) to reduce the high frequency noise and were segmented using a single-level, global threshold (330/1000) based on a visual inspection of each specimen. Four individual regions from the same specimen had an adapted threshold (350/1000) after visually checking the segmented scan images. A despeckle algorithm was applied to remove isolated bone regions with a volume lower than 10 voxels. BV/TV was determined by dividing the number of bone voxels (BV) by the total number of voxels in the region of interest (TV). Trabecular microstructure (Tb.N, Tb.Th and Tb.Sp) were calculated using the distance transformation method, where maximal spheres are filled into the segmented image [35]. Examples of the HR-pQCT and micro-CT scans segmentation are presented in Fig. 2.

2.6. Statistical analysis

Statistical analyses were completed in GraphPad Prism (7.0, GraphPad Software: La Jolla California, USA) and R Studio (1.0.44: Boston, USA). A $p < 0.05$ indicated statistical significance, unless stated otherwise. Morphometric measurements were non-normally distributed following visual and statistical checks (Shapiro-Wilk test), therefore median and interquartile ranges were calculated for each measurement. Wilcoxon-Rank tests were performed to compare the paired HR-pQCT and micro-CT scans (IS100, IS150, IS200, EV100 *vs.* micro-CT). Friedman's test with post-hoc between-pair analyses using Dunn's multiple comparisons tests was performed to compare the four HR-pQCT scans.

Linear regression analyses were performed to evaluate the correlation between the measurements performed on the HR-pQCT and micro-CT images; coefficient of determination (r^2), equation slope and intercept, root mean square error (RMSE) and the largest difference between the predicted and morphological parameters (max. error) were calculated. A region was treated as an outlier and removed from the regression analyses if all comparisons (IS100, IS150, IS200 and EV100) exceeded the Cook's distance (4/number of regions). Regression slopes were compared between the HR-pQCT scans using a one-way ANOVA and *t*-tests with Bonferroni corrections, to account for multiple tests *i.e.* between scan conditions (0.05/4) and between regions (0.05/3).

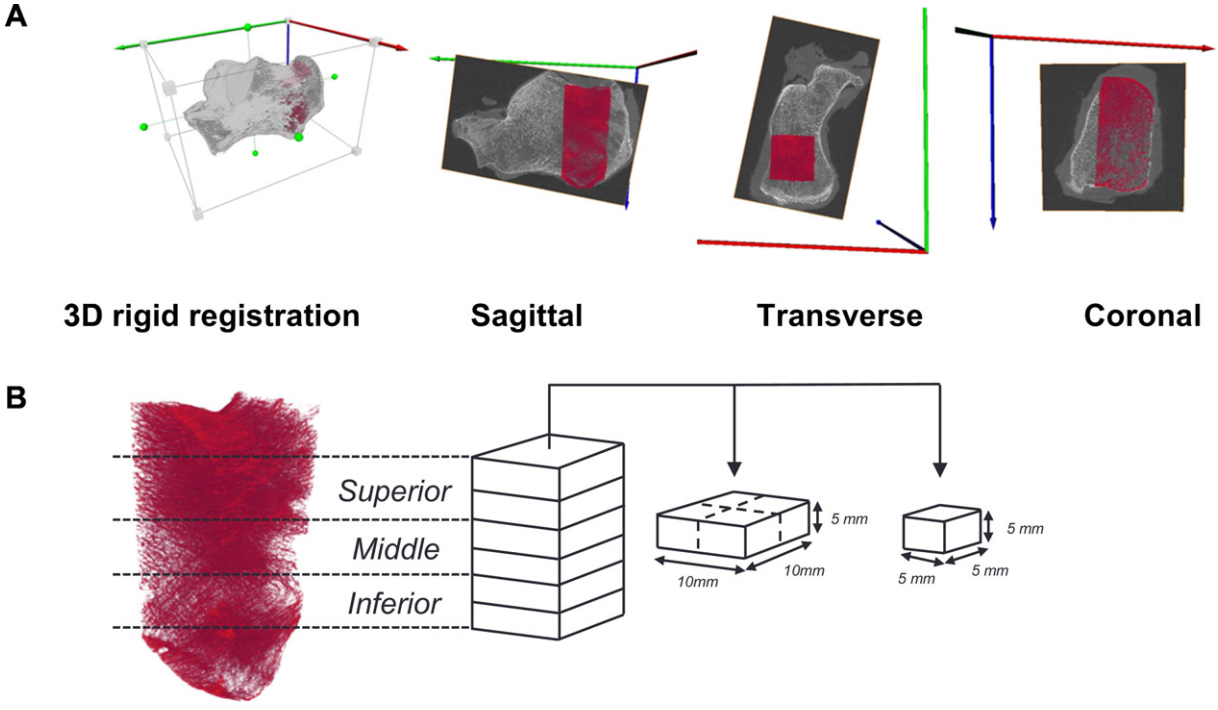

Fig. 1. Methodology for registration and identifying the cubed regions of interest for HR-pQCT and micro-CT image analysis. A) The HR-pQCT images were rigidly registered to the micro-CT image (red). Examples of the micro-CT and HR-pQCT images following transformation are shown in all 3 planes (sagittal, transverse and coronal). B) Scans were split into six 10 × 10 × 5 mm regions along the superior-inferior axis. The 6 regions were sub-divided into four equal sized cubed volumes of interest (5 × 5 × 5 mm), which were used in the evaluations. Two of the 10 × 10 × 5 mm regions were combined into superior, middle and inferior regions: there were eight 5 × 5 × 5 mm-cubed volumes of interest in these regions. Superior = region 1 to 8; middle = region 9 to 16; inferior = region 17 to 24.

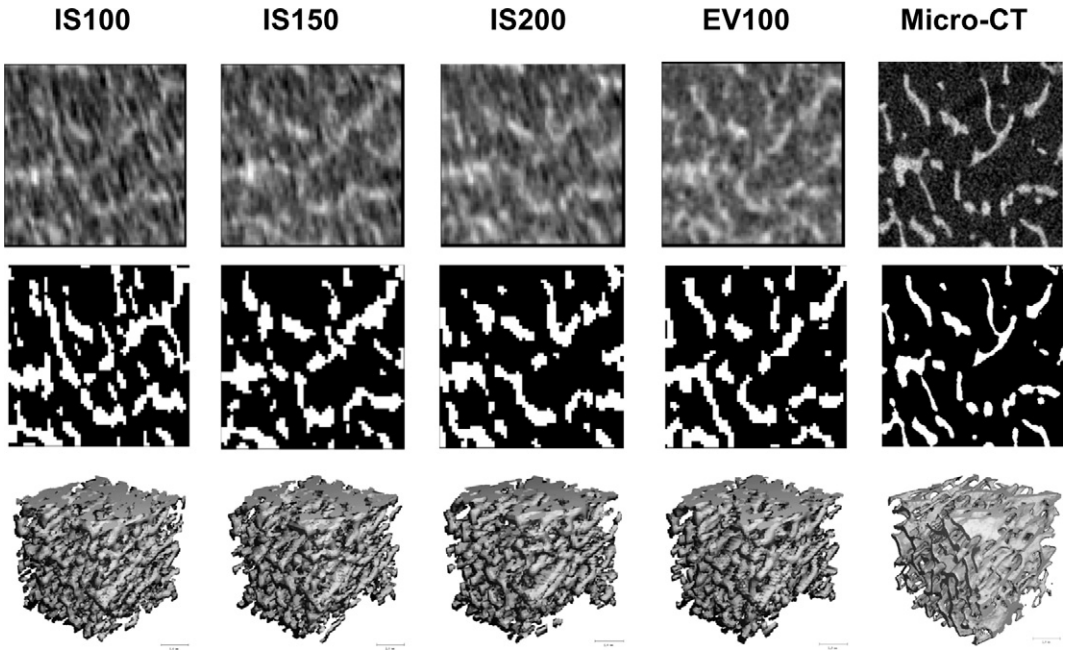

Fig. 2. Segmentation of representative regions of interest in the calcaneus using HR-pQCT and micro-CT. A slice is shown for a representative HR-pQCT and micro-CT image. The HR-pQCT scan is separated into the condition (*in situ* (IS) and *ex vivo* (EV)) and scan integration time (100, 150 and 200 ms). This includes a grayscale and segmented slice, and the 3D volume of interest.

Bland-Altman methods were performed to test for bias (mean ± SD) between the paired HR-pQCT scans and the micro-CT scan [36].

3. Results

3.1. Descriptive comparisons

In total, 108 matched regions were evaluated between all HR-pQCT scans and the micro-CT scans, after removal of HR-pQCT scans with visible air bubbles or negative Tb.vBMD values. Table 1 contains the descriptive statistics for the morphological measurements from the scans. All estimates of BV/TV^d, Tb.Th^d and Tb.Sp^d derived from HR-pQCT images (IS100, IS150, IS200 and EV100) were significantly lower than the corresponding measures obtained from micro-CT images (all $p < 0.001$). In contrast, Tb.N measured in all HR-pQCT images was significantly overestimated ($p < 0.001$) when compared to the micro-CT measurements. No differences were found among the Tb.vBMD and BV/TV^d measurement performed on the *in situ* HR-pQCT images across the 3 integration times, but Tb.N, Tb.Th^d and Tb.Sp^d measured from IS100, IS150 and IS200 images were all significantly different to one another ($p < 0.001$); as the integration time increased, Tb.N decreased and Tb.Th^d and Tb.Sp^d increased. Tb.vBMD, BV/TV^d and Tb.N measured from the *in situ* HR-pQCT images were significantly higher, and Tb.Sp^d was significantly lower, compared to the measurements from the EV100 HR-pQCT image ($p < 0.001$). Tb.Th^d measured from the IS100 and IS150 was significantly lower than measurements from the EV100 HR-pQCT image ($p < 0.001$), but there was no difference between the IS200 and EV100 measurement ($p > 0.99$).

3.2. Regression analyses in the common whole sample

Regression analyses for all evaluable regions are shown in Table 2. There were strong correlations between BV/TV measured in the micro-CT images and BV/TV^d computed from both *in situ* and *ex vivo*

Table 1
Descriptive statistics for the micro-CT and HR-pQCT scan images.

Measurements	Micro-CT	HR-pQCT			
		IS200	IS150	IS100	EV100
Tb.vBMD (mg HA/cm^3)	-	102^c (64, 132)	104^c (67, 127)	104^c (64, 131)	99 (61, 132)
BV/TV (%)	**13.6 (10.2, 16.2)**	8.7^c (5.4, 10.7)	8.7^c (5.5, 10.6)	8.7^c (5.4, 10.9)	8.2 (5, 11)
Tb.N (mm^{-1})	**1.49 (1.37, 1.62)**	1.98^c (1.72, 2.44)	2.14^{bc} (1.84, 2.89)	2.51^{abc} (2.24, 3.32)	1.79 (1.48, 1.97)
Tb.Th (mm)	**0.128 (0.119, 0.135)**	0.044 (0.028, 0.053)	0.040^{bc} (0.025, 0.05)	0.034^{abc} (0.02, 0.046)	0.046 (0.029, 0.056)
Tb.Sp (mm)	**0.64 (0.56, 0.7)**	0.46^c (0.38, 0.55)	0.42^{bc} (0.33, 0.49)	0.36^{abc} (0.28, 0.41)	0.51 (0.45, 0.62)

Abbreviations: *in situ* 100 ms (IS100); *in situ* 150 ms (IS150); *in situ* 200 ms (IS200); *ex vivo* 100 ms (EV100); trabecular vBMD (Tb.vBMD), bone volume fraction (BV/TV), trabecular number (Tb.N), trabecular thickness (Tb.Th), trabecular spacing (Tb.Sp).
$N = 108$ matched regions. Data are presented as median (25%, 75% percentile). Shaded areas indicate measurements that were directly measured.
Measurements in bold are significantly different to all HR-pQCT scans (all $p < 0.001$).
$p < 0.001$ compared to [a] IS150, [b] IS200 and [c] EV100.

Table 2
Regression analysis for the HR-pQCT *vs.* micro-CT trabecular measurement across all regions.

Sample	r^2	Intercept	Slope	RMSE	Max. error
Bone volume/total volume^d (1) ($n = 104$)					
IS200	0.96	0.050	1.000	0.009	0.021
IS150	0.95	0.050	1.010	0.009	0.023
IS100	0.96	0.050	1.000	0.008	0.020
EV100	0.98	0.053	1.020	0.008	0.014
Trabecular number (mm^{-1}) ($n = 106$)					
IS200	0.61	0.805	0.347§	0.15	0.46
IS150	0.44	0.921	0.263§	0.18	0.59
IS100	0.33	0.941	0.217*,§	0.19	0.67
EV100	0.79	0.678	0.469	0.11	0.30
Trabecular thickness^d (mm) ($n = 107$)					
IS200	0.55	0.103	0.588	0.009	0.025
IS150	0.53	0.104	0.607	0.010	0.026
IS100	0.55	0.106	0.663	0.009	0.023
EV100	0.59	0.102	0.586	0.008	0.022
Trabecular spacing^d (mm) (n = 107)					
IS200	0.55	0.367	0.556	0.07	0.21
IS150	0.43	0.401	0.530	0.08	0.23
IS100	0.33	0.402	0.627	0.09	0.24
EV100	0.66	0.348	0.517	0.06	0.21

Abbreviations: *in situ* 100 ms (IS100); *in situ* 150 ms (IS150); *in situ* 200 ms (IS200); *ex vivo* 100 ms (EV100); RMSE, root mean square error; max. error, maximum error from the regression equation.
All r^2 values are statistically significant, $p < 0.001$. Comparison of the regression slopes between different HR-pQCT conditions: * $p < 0.01$ compared to IS200; § $p < 0.001$ compared to EV100.

HR-pQCT images ($r^2 = 0.95$–0.98). There was no difference between the BV/TV *versus* BV/TV^d regression slopes ($p = 0.94$) and the RMSEs were similar (0.8–0.9%). The BV/TV^d maximum errors obtained from the *in situ* HR-pQCT images were similar (2–2.3%), and the value measured from the *ex vivo* HR-pQCT image was apparently lower (1.4%).

Weak to moderate correlations were found between Tb.N measured in the micro-CT and the *in situ* HR-pQCT images; the correlations were dependent on integration time ($r^2 = 0.33$ for IS100 and $r^2 = 0.61$ for IS200) with significant differences between the IS100 and IS200 regression slopes ($p < 0.01$). There seemed to be lower RMSE and maximum error when the *in situ* integration time was increased from IS100 to IS200 (0.19 to 0.15 mm^{-1} and 0.67 to 0.46 mm^{-1}, respectively). The Tb.N correlation improved further when measured by the *ex vivo* HR-pQCT image in comparison to the micro-CT image ($r^2 = 0.79$) and the regression slope was significantly different to that obtained with the *in situ* comparisons (IS100, IS150 and IS200, $p < 0.001$). Tb.N measured from the *ex vivo* HR-pQCT image also seemed to have lower RMSE (0.11 mm^{-1}) and maximum error (0.30 mm^{-1}) compared measurements from the *in situ* HR-pQCT images.

Moderate correlations were found for Tb.Th^d estimated in all HR-pQCT images with respect to the respective micro-CT measurements ($r^2 = 0.53$–0.59). There were no significant differences between the Tb.Th^d regression slopes ($p = 0.73$), and the RMSE and maximum error were all similar between the different HR-pQCT integration times. Weak to moderate correlations were found for Tb.Sp^d estimated in all HR-pQCT images with respect to Tb.Sp micro-CT measurements; *in situ* correlations were dependent on the integration time ($r^2 = 0.33$ for IS100 and $r^2 = 0.55$ for IS200) and the correlation was found to increase when measured in the *ex vivo* HR-pQCT image ($r^2 = 0.66$). There were no differences in Tb.Sp^d regression slopes ($p = 0.64$), and the Tb.Sp^d RMSE and maximum error were all similar.

3.3. Regression analysis in superior, middle and inferior regions of the calcaneus

We completed a regional analysis by grouping the 5 mm^3 regions of interests into superior, middle and inferior regions of the calcaneal samples (Fig. 1). A number of cubed regions from the inferior region were removed as the analysis returned a negative vBMD. The results within each of these regions for BV/TV^d and Tb.N, the measurements used to compute Tb.Th^d and Tb.Sp^d from the HR-pQCT images, are shown in Tables 3 and 4, respectively, with corresponding regression plots in the Supplemental material 2. Data for Tb.Th^d and Tb.Sp^d are shown in the Supplemental materials 2 to 4.

BV/TV measured by micro-CT or BV/TV^d estimated by HR-pQCT were highest in the superior region of the calcaneus in comparison to the middle and inferior regions ($p < 0.01$ for all images), but were not statistically significant between the middle and inferior regions (micro-CT, $p = 0.13$; HR-pQCT, $p = 0.16$–0.29)(Table 3). There were strong correlations at the superior, middle and inferior regions for BV/TV measured in the micro-CT images and BV/TV^d computed from both *in situ* and *ex vivo* HR-pQCT images ($r^2 = 0.96$–0.99, all $p < 0.001$). The superior and middle region regression slopes for BV/TV^d were significantly different to the inferior region, within each respective integration time *in situ* ($p < 0.017$). The BV/TV^d RMSE was below 1% in all regions. The maximum error was 1–2% for the *in situ* and *ex vivo* HR-pQCT images at the superior, middle and inferior regions.

Tb.N measured by micro-CT was significantly higher in the superior and middle region compared to the inferior region ($p = 0.02$ and $p = 0.03$, respectively)(Table 4). A similar relationship was found for Tb.N measured from the *ex vivo* HR-pQCT images ($p = 0.003$ and $p = 0.005$, respectively). In contrast, Tb.N measured from the *in situ* images appeared to increase from the superior to inferior region, though these values were largely not significantly different between the regions, apart from Tb.N being significantly higher in the inferior region compared to the superior region in the IS100 HR-pQCT images ($p = 0.03$).

The correlation for Tb.N measured from micro-CT and HR-pQCT images was strongest in the superior region ($r^2 = 0.70$–0.93, all $p < 0.001$) compared to the middle region ($r^2 = 0.52$–0.76, all $p < 0.001$). No correlation was found for Tb.N in the inferior region (all $p \geq 0.21$). The strongest correlations were found for Tb.N measured in the *ex vivo* HR-pQCT compared to the micro-CT image, and was the only HR-pQCT image to be significantly, albeit moderately, correlated with micro-CT in the inferior region. All superior region regression slopes

Table 3
Bone volume fraction regression data for the different HR-pQCT conditions at the three different regions.

Sample	Median (IQR)	r^2	Intercept	Slope	RMSE	Max. error
Superior ($n = 42$)						
Micro-CT	0.159 (0.139, 0.187)					
IS200	0.105 (0.081, 0.126)	**0.96**	0.069	0.862§	0.009	0.018
IS150	0.103 (0.083, 0.124)	**0.96**	0.070	0.857§	0.009	0.019
IS100	0.105 (0.084, 0.124)	**0.97**	0.066	0.880§	0.008	0.019
EV100	0.102 (0.082, 0.130)	**0.97**	0.063	0.927*,§	0.007	0.020
Middle ($n = 43$)						
Micro-CT	0.125 (0.097, 0.153)					
IS200	0.078 (0.046, 0.103)	**0.96**	0.053	0.954§	0.007	0.020
IS150	0.077 (0.046, 0.102)	**0.96**	0.052	0.962§	0.008	0.022
IS100	0.077 (0.044, 0.100)	**0.96**	0.053	0.967§	0.007	0.021
EV100	0.071 (0.044, 0.095)	**0.99**	0.051	1.030	0.004	0.013
Inferior ($n = 21$)						
Micro-CT	0.100 (0.075, 0.123)					
IS200	0.056 (0.036, 0.075)	**0.98**	0.035	1.160	0.005	0.010
IS150	0.058 (0.036, 0.075)	**0.98**	0.033	1.180	0.005	0.012
IS100	0.056 (0.035, 0.074)	**0.98**	0.035	1.160	0.005	0.010
EV100	0.050 (0.025, 0.071)	**0.99**	0.049	1.070	0.004	0.008

Abbreviations: *in situ* 100 ms (IS100); *in situ* 150 ms (IS150); *in situ* 200 ms (IS200); *ex vivo* 100 ms (EV100); RMSE, root mean square error; max. error, maximum error from the regression equation.
Median (interquartile range) bone volume fraction (1) is presented within each integration time at each region.
r^2 values in bold are statistically significant, $p < 0.001$. Comparison of the regression slopes between the regions, within the same integration time: * $p < 0.017$ compared to the middle region; § $p < 0.017$ compared to the inferior region.

Table 4
Trabecular number regression data for the different HR-pQCT conditions at the three different regions.

Sample	Median (IQR)	r^2	Intercept	Slope	RMSE	Max. error
Superior ($n = 41$)						
Micro-CT	1.51 (1.37, 1.65)					
IS200	1.87 (1.64, 2.10)	**0.88**	0.565	0.499*,§	0.10	0.20
IS150	2.02 (1.79, 2.28)	**0.82**	0.601	0.454*,§	0.12	0.28
IS100	2.36 (1.95, 2.59)	**0.70**	0.632	0.385§	0.16	0.38
EV100	1.81 (1.55, 1.98)	**0.93**	0.461	0.584*,§	0.07	0.17
Middle ($n = 44$)						
Micro-CT	1.56 (1.37, 1.67)					
IS200	1.99 (1.67, 2.56)	**0.70**	0.860	0.317§	0.12	0.27
IS150	2.13 (1.89, 2.96)	**0.59**	0.916	0.264§	0.15	0.35
IS100	2.49 (2.29, 3.44)	**0.52**	0.822	0.258§	0.16	0.38
EV100	1.86 (1.51, 2.07)	**0.76**	0.680	0.460§	0.11	0.24
Inferior (n = 21)						
Micro-CT	1.45 (1.32, 1.47)					
IS200	2.06 (1.88, 2.36)	0.00	1.430	−0.013	0.10	0.22
IS150	2.34 (2.19, 2.85)	**0.05**	1.510	−0.044	0.10	0.21
IS100	2.87 (2.61, 3.30)	**0.08**	1.560	−0.054	0.10	0.20
EV100	1.69 (1.13, 1.79)	**0.50**	1.110	0.196	0.07	0.20

Abbreviations: *in situ* 100 ms (IS100); *in situ* 150 ms (IS150); *in situ* 200 ms (IS200); *ex vivo* 100 ms (EV100); RMSE, root mean square error; max. error, maximum error from the regression equation.
Median (interquartile range) trabecular number (mm^{-1}) is presented within each integration time at each region.
r^2 values in bold are statistically significant, $p \le 0.001$. Comparison of the regression slopes between the regions, within the same integration time: * $p < 0.017$ compared to the middle region; § $p < 0.017$ compared to the inferior region.

were significantly different to the middle (apart from IS100) and inferior regions, within each respective integration time. All middle region regression slopes were also significantly different to the inferior region, within each respective integration time. A lower RMSE and maximum error were apparent at the superior and middle region with increasing integration time *in situ*, but this was not apparent at the inferior region *in situ*.

3.4. Bland-Altman method comparison

Bland-Altman plots for measurements in the superior, middle and inferior regions are presented for BV/TV^d and Tb.N in Fig. 3. Plots for $Tb.Th^d$ and $Tb.Sp^d$ are available in the supplemental material 5. BV/TV^d computed from the HR-pQCT images underestimated BV/TV measured by micro-CT. The mean biases for the *in situ* and *ex vivo* HR-pQCT images were similar between the integration times and regions: approximately 4 to 5%. Tb.N measured by HR-pQCT images systematically overestimated Tb.N measured from the micro-CT images. The mean bias for Tb.N decreased as the integration time increased in the *in situ* HR-pQCT images at all regions. The Tb.N mean bias was lower in the *ex vivo* HR-pQCT images compared to the *in situ* HR-pQCT images. The mean bias (±SD) for IS100 and IS150 increased from the superior to inferior regions (IS100: superior = $-0.85 \pm 0.40\ mm^{-1}$, inferior = $-1.46 \pm 0.55\ mm^{-1}$; IS150: superior = $-0.56 \pm 0.33\ mm^{-1}$, inferior = $-0.98 \pm 0.53\ mm^{-1}$), whereas the mean bias for IS200 increased from the superior to middle regions and was similar for the middle to inferior regions (superior = $-0.44 \pm 0.28\ mm^{-1}$, middle = $-0.58 \pm 0.42\ mm^{-1}$, inferior = $-0.63 \pm 0.41\ mm^{-1}$).

4. Discussion

This study describes the novel adaptation of HR-pQCT for the measurement of calcaneal BV/TV^d and microstructure. Calcaneus BV/TV^d and microstructure assessed at an isotropic 82 μm voxel size was validated against micro-CT at an isotropic 17 μm voxel size, which acted as a 'gold-standard' reference. HR-pQCT BV/TV^d had a strong correlation across all scan conditions, explaining 95 to 98% of micro-CT BV/TV, when all regions were combined. This is important, as BV/TV^d is a key measurement to predict bone strength [21,22,37] and has a strong association with fracture risk [4,6].

The strong correlation and underestimation of BV/TV^d that was found with the calcaneus HR-pQCT scan images was consistent with previous studies at the distal radius and distal tibia [22–24]. The lower estimation of BV/TV^d, derived from Tb.vBMD measurement by HR-pQCT, could be caused by the global threshold used to define bone tissue and lower signal-to-noise ratio resulting in a higher number of partial volume voxels in the HR-pQCT images compared to the micro-CT images. It should also be remembered that the HR-pQCT measurements were made in the intact bone, so that beam hardening artifacts caused by the intact cortex and surrounding bone structures may have also impacted on Tb.vBMD measurement [38]. Trabecular vBMD was similar at the different integration times. On removing the calcaneus from the foot, the trabecular vBMD and BV/TV^d were significantly lower than the *in situ* scans, even though the absolute difference was relatively small. Dissection may have exposed the calcaneus to air bubbles that were undetectable in the HR-pQCT images, or else there may have been a reduction in image noise with removal of the surrounding bones and soft tissue. Nonetheless, a regression equation that is independent of integration time can be used to adjust calcaneus BV/TV^d computed from HR-pQCT images to that measured by micro-CT ($Y = 1.010^*X + 0.050$).

Calcaneus Tb.N was systematically overestimated, and $Tb.Th^d$ and $Tb.Sp^d$ subsequently underestimated when measured by HR-pQCT using the standard patient analysis, consistent with previous studies at the radius and tibia [22–24]. It has been well established that the accurate measurement of trabecular microstructure is dependent on the spatial resolution [23], which was equivalent to the calcaneus Tb.Th measured by micro-CT in the current study. The higher values of Tb.N in purely trabecular samples measured by HR-pQCT compared to micro-CT are in keeping with previous reports [22,23], probably reflecting factors such as decreased signal-to-noise ratio and partial volume effects; factors that are exacerbated at the shorter integration times as observed in our study. A similar increase in Tb.N for individual specimens has been reported when comparing a 123 μm to 82 μm isotropic voxel size [23]. BV/TV^d may be less susceptible to such factors as it is derived from Tb.vBMD, in which the averaging per cm^{-3} is likely to suppress differences between integration times, as has been demonstrated with direct BV/TV measurement [21,25,39].

The direct measurement of Tb.N is fundamental to determining $Tb.Sp^d$ and $Tb.Th^d$ using plate-model assumptions. The HR-pQCT indirect patient analysis aims to preserve all trabeculae using a low global threshold in order to measure Tb.N [40]. The caveat is that if an image has a low signal-to-noise ratio, image noise could be categorized as bone following application of the HR-pQCT threshold to segment to bone and marrow phases [31]; this is the possible mechanism of the greater overestimation of Tb.N at lower integration times and in the inferior regions of the calcaneus. Increasing integration time improved the accuracy of Tb.N in comparison to micro-CT, leading also to an improvement in $Tb.Sp^d$ accuracy. However, $Tb.Th^d$ was not improved, due to its equal-weighted dependency on BV/TV^d and Tb.N. Weak correlations with $Tb.Th^d$ have been confirmed in studies at the radius and tibia despite strong correlations for BV/TV^d and Tb.N [23,24]; this study therefore further highlights a limitation in the use of the plate-model assumptions using the first generation XtremeCT. A better signal-to-noise ratio, provided by a higher Tb.BMD, was also reflected in the improved accuracy of Tb.N in the denser superior region of the calcaneus than in the middle and, particularly, inferior regions. Furthermore, the regions with thinner trabeculae (middle and inferior) could be more susceptible to errors with the global threshold applied by the indirect HR-pQCT analysis, which could also explain differences in trabecular measurement accuracy compared to other studies [21–24,40]. Other thresholds may improve the accuracy; for example, in femoral head trabecular bone

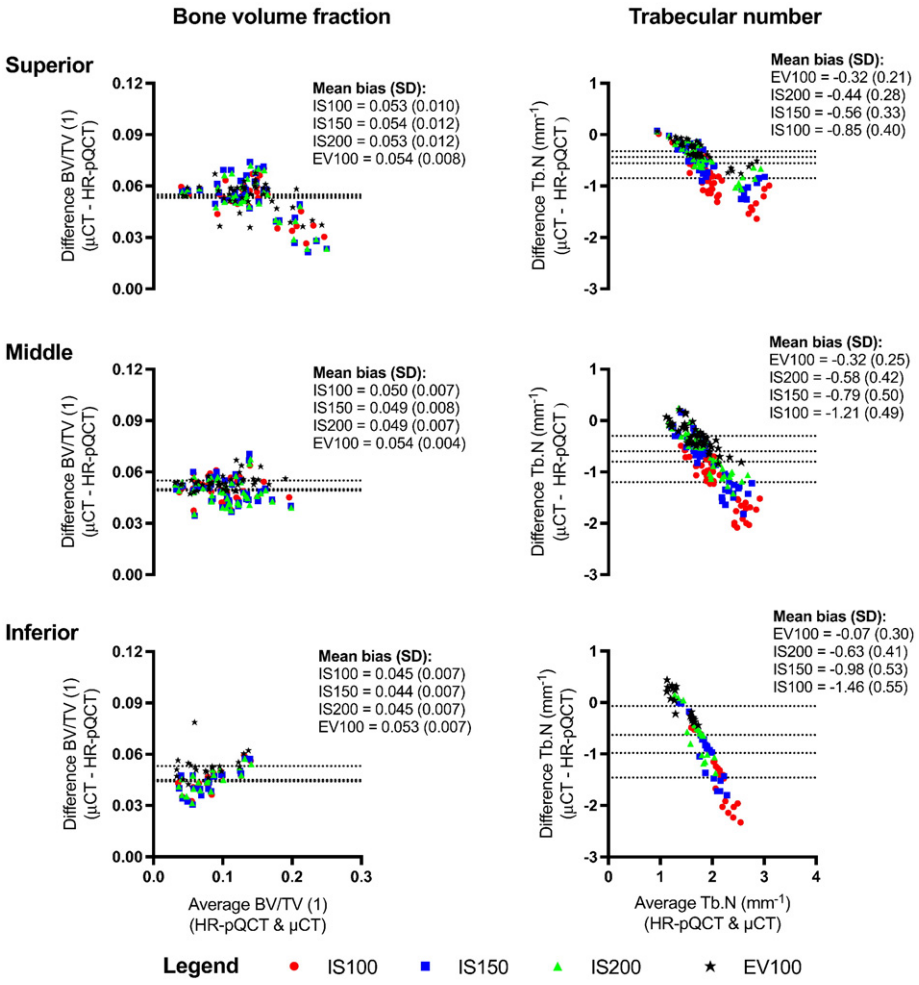

Fig. 3. Bland-Altman plots for calcaneus bone volume fraction and trabecular number measured from HR-pQCT images (IS100, IS150 and IS200, and EV100) compared to micro-CT image at different regions (superior, middle and inferior). Abbreviations: *in situ* 100 ms (IS100); *in situ* 150 ms (IS150); *in situ* 200 ms (IS200); *ex vivo* 100 ms (EV100).

samples a local-derived direct assessment improved estimates of trabecular thickness and spacing, though the overall impact was relatively small [40].

The superior region scanned at 200 ms integration time had comparable correlation, slopes and accuracy for BV/TV^d, Tb.N and $Tb.Sp^d$ compared to previous studies at the distal radius and distal tibia [22–24]. This is encouraging, as these validated protocols have been widely used in clinical studies [4–9]. In addition to lower bone volume in the middle and inferior regions, the signal-to-noise ratios may also be impacted by the surrounding bones of the foot at these levels in affecting the measurement of trabecular microstructure using HR-pQCT. The more marked differences in Tb.N between the *in situ* and *ex vivo* scans at the inferior region suggest that this may be the case. In the same region, noise is likely to have contributed to the fact that although the *ex vivo* scan had similar Tb.N values to the micro-CT, the correlation was still relatively weak. Additionally, the poorer estimation at these regions could be due to thinner trabeculae, which has been highlighted as an issue in a previous study comparing plate- and rod-like trabeculae at different voxel sizes [41].

The results reinforce using 200 ms integration time for the calcaneus HR-pQCT scans to compensate for the X-ray absorption from the surrounding tissues. Practically, there would still be a low radiation exposure per 110 slices (6 µSv per scan). However, scan duration would be 4.2 min (per 110 slices using the XtremeCT I), which is longer than the distal radius and distal tibia scans (2.8 min). This would increase the probability of participant movement and may consequently affect measurement precision error. Precision error of HR-pQCT measurements at the calcaneus has not been established *in vivo*. Distal radius and tibia error is already between 3 and 6% (least significant change 8 to 17%) for trabecular microstructure using rigid registration at 100 ms integration time [42–44]. However, it can be questioned whether the accuracy at lower integration times could be accepted to improve reproducibility, which could be the case if BV/TV^d, and possibly other volumetric measurements, were of primary interest. The comparison of different integration times *in vivo* therefore requires investigation.

We have attempted to best represent *in vivo* conditions by obtaining HR-pQCT scans *in situ*, with bones, soft tissue and marrow intact, to inform the clinical translation of the method. However, we recognize there are several limitations to the study. First, and as has been discussed, the study was free from movement artifact, which would be expected to affect measurement accuracy *in vivo*. Second, measurements may have been impacted by the deterioration of bone mineral given the advanced age of the donors. We found that BV/TV measured by micro-CT was comparable to previous studies that have evaluated similar regions and specimens of a similar age and gender [20,45,46]; preliminary *in vivo* HR-pQCT measurements suggest derived BV/TVs of up to 26% (unpublished data) and this is likely to be greater in a younger cohort. Assessment of calcaneus cortical bone was not undertaken due to the extremely thin cortices observed in our cohort that affected the segmentation of the calcaneus cortical bone; whether this would be possible in younger specimens remains to be determined. Third, in an attempt to broaden the BV/TV range that was validated, we evaluated smaller cubic regions of interest [25,30], potentially increasing errors between modalities that

would have been lessened by comparisons of larger cross-sectional area. Fourth, micro-CT analysis primarily used a fixed threshold, which was adapted for 4 regions (same specimen). Others have used an adaptive threshold for all samples [23] and this may be a factor in differences between the studies. Finally, we used the first generation XtremeCT device (isotropic voxel size = 82 μm, spatial resolution = 127 to 154 μm [47]) that uses plate model-assumptions to compute trabecular microstructure. The second generation XtremeCT device has a reported superior spatial resolution (isotropic voxel size = 61 μm, spatial resolution = 95 μm), which includes more independent measurements and may improve the direct estimation of trabecular microstructure [48]. Furthermore, the field of view is slightly larger and the scan time is shorter, which may better accommodate the quantification of calcaneus trabecular microstructure *in vivo*.

5. Conclusion

In summary, we have developed a protocol to scan the calcaneus using HR-pQCT that has achieved measurement correlation and accuracy comparable to previous validation studies performed at the distal radius and distal tibia. Here, scanning a superior region of the bone with a 200 ms scan integration time for the quantification of trabecular microstructure is preferred, based on the proposed protocol and integration times investigated in this study. Investigating inferior regions of the calcaneus and using lower integration time appears inaccurate. Future developments will include the testing of HR-pQCT integration times *in vivo* and determining measurement precision error, bearing in mind the potential for movement artifacts in longer scan durations. Such studies will determine whether calcaneus HR-pQCT scans could have a significant clinical utility in osteoporosis or podiatry research.

Disclosures

LMM, ED, MAP, JRR, GJK and EVM have nothing to declare. NV is an employee of SCANCO Medical AG.

Acknowledgements

We acknowledge the technical assistance provided by Skelet.AL (University of Sheffield) in performing the micro-CT scans. We acknowledgement funding from the MRC and Arthritis Research UK as part of the MRC–Arthritis Research UK Centre for Integrated Research into Musculoskeletal Ageing (MR/K006312/1) and the EPSRC Frontier grant MULTISIM (EP/K03877X/1).

Appendix A. Supplementary data

Supplementary data to this article can be found online at https://doi.org/10.1016/j.bone.2017.09.013.

References

[1] Consensus development conference: diagnosis, prophylaxis, and treatment of osteoporosis, Am. J. Med. 94 (6) (1993) 646–650.
[2] J.A. Kanis, O. Johnell, A. Oden, H. Johansson, E. McCloskey, FRAX and the assessment of fracture probability in men and women from the UK, Osteoporos. Int. 19 (4) (2008) 385–397.
[3] K. Engelke, J.E. Adams, G. Armbrecht, P. Augat, C.E. Bogado, M.L. Bouxsein, D. Felsenberg, M. Ito, S. Prevrhal, D.B. Hans, E.M. Lewiecki, Clinical use of quantitative computed tomography and peripheral quantitative computed tomography in the management of osteoporosis in adults: the 2007 ISCD official positions, Journal of clinical densitometry: the official journal of the International Society for Clinical Densitometry 11 (1) (2008) 123–162.
[4] M.H. Edwards, D.E. Robinson, K.A. Ward, M.K. Javaid, K. Walker-Bone, C. Cooper, E.M. Dennison, Cluster analysis of bone microarchitecture from high resolution peripheral quantitative computed tomography demonstrates two separate phenotypes associated with high fracture risk in men and women, Bone 88 (2016) 131–137.
[5] J. Wang, E.M. Stein, B. Zhou, K.K. Nishiyama, Y.E. Yu, E. Shane, X.E. Guo, Deterioration of trabecular plate-rod and cortical microarchitecture and reduced bone stiffness at distal radius and tibia in postmenopausal women with vertebral fractures, Bone 88 (2016) 39–46.
[6] N. Vilayphiou, S. Boutroy, P. Szulc, B. van Rietbergen, F. Munoz, P.D. Delmas, R. Chapurlat, Finite element analysis performed on radius and tibia HR-pQCT images and fragility fractures at all sites in men, J. Bone Miner. Res. 26 (5) (2011) 965–973.
[7] J.N. Tsai, A.V. Uihlein, S.M. Burnett-Bowie, R.M. Neer, N.P. Derrico, H. Lee, M.L. Bouxsein, B.Z. Leder, Effects of two years of teriparatide, denosumab, or both on bone microarchitecture and strength (DATA-HRpQCT study), J. Clin. Endocrinol. Metab. 101 (5) (2016) 2023–2030.
[8] H.M. Macdonald, K.K. Nishiyama, D.A. Hanley, S.K. Boyd, Changes in trabecular and cortical bone microarchitecture at peripheral sites associated with 18 months of teriparatide therapy in postmenopausal women with osteoporosis, Osteoporos. Int. 22 (1) (2011) 357–362.
[9] S. Hansen, E.M. Hauge, J.-E.B. Jensen, K. Brixen, Differing effects of PTH 1–34, PTH 1–84, and zoledronic acid on bone microarchitecture and estimated strength in postmenopausal women with osteoporosis: an 18-month open-labeled observational study using HR-pQCT, J. Bone Miner. Res. 28 (4) (2013) 736–745.
[10] C. Barnabe, H. Buie, M. Kan, E. Szabo, S.G. Barr, L. Martin, S.K. Boyd, Reproducible metacarpal joint space width measurements using 3D analysis of images acquired with high-resolution peripheral quantitative computed tomography, Med. Eng. Phys. 35 (10) (2013) 1540–1544.
[11] W. Srikhum, W. Virayavanich, A.J. Burghardt, A. Yu, T. Link, J.B. Imboden, X. Li, Quantitative and semiquantitative bone erosion assessment on high-resolution peripheral quantitative computed tomography in rheumatoid arthritis, J. Rheumatol. 40 (4) (2013) 408–416.
[12] A. Kroker, Y. Zhu, S.L. Manske, R. Barber, N. Mohtadi, S.K. Boyd, Quantitative in vivo assessment of bone microarchitecture in the human knee using HR-pQCT, Bone 97 (2017) 43–48.
[13] M.L. Bouxsein, S.E. Radloff, Quantitative ultrasound of the calcaneus reflects the mechanical properties of calcaneal trabecular bone, J. Bone Miner. Res. 12 (5) (1997) 839–846.
[14] C.F. Njeh, T. Fuerst, E. Diessel, H.K. Genant, Is quantitative ultrasound dependent on bone structure? A reflection, Osteoporos. Int. 12 (1) (2001) 1–15.
[15] A. Moayyeri, J.E. Adams, R.A. Adler, M.A. Krieg, D. Hans, J. Compston, E.M. Lewiecki, Quantitative ultrasound of the heel and fracture risk assessment: an updated meta-analysis, Osteoporos. Int. 23 (1) (2012) 143–153.
[16] M.L. Frost, G.M. Blake, I. Fogelman, Changes in QUS and BMD measurements with antiresorptive therapy: a two-year longitudinal study, Calcif. Tissue Int. 69 (3) (2014) 138–146.
[17] M.A. Paggiosi, R. Barkmann, C.C. Gluer, C. Roux, D.M. Reid, D. Felsenberg, M. Bradburn, R. Eastell, A European, Multicenter comparison of quantitative ultrasound measurement variables: the OPUS study, Osteoporos. Int. 23 (12) (2012) 2815–2828.
[18] M. Qiang, Y. Chen, K. Zhang, H. Li, H. Dai, Measurement of three-dimensional morphological characteristics of the calcaneus using CT image post-processing, J Foot Ankle Res 7 (19) (2014) 1–9.
[19] T.M. Malaquias, C. Silveira, W. Aerts, F. De Groote, G. Dereymaeker, J. Vander Sloten, I. Jonkers, Extended foot-ankle musculoskeletal models for application in movement analysis, Comput Methods Biomech Biomed Engin 20 (2) (2017) 153–159.
[20] G. Diederichs, T.M. Link, M. Kentenich, K. Schwieger, M.B. Huber, A.J. Burghardt, S. Majumdar, P. Rogalla, A.S. Issever, Assessment of trabecular bone structure of the calcaneus using multi-detector CT: correlation with microCT and biomechanical testing, Bone 44 (5) (2009) 976–983.
[21] B. Zhou, J. Wang, Y.E. Yu, Z. Zhang, S. Nawathe, K.K. Nishiyama, F.R. Rosete, T.M. Keaveny, E. Shane, X.E. Guo, High-resolution peripheral quantitative computed tomography (HR-pQCT) can assess microstructural and biomechanical properties of both human distal radius and tibia: ex vivo computational and experimental validations, Bone 86 (2016) 58–67.
[22] X.S. Liu, X.H. Zhang, K.K. Sekhon, M.F. Adams, D.J. McMahon, J.P. Bilezikian, E. Shane, X.E. Guo, High-resolution peripheral quantitative computed tomography can assess microstructural and mechanical properties of human distal tibial bone, J. Bone Miner. Res. 25 (4) (2010) 746–756.
[23] W. Tjong, G.J. Kazakia, A.J. Burghardt, S. Majumdar, The effect of voxel size on high-resolution peripheral computed tomography measurements of trabecular and cortical bone microstructure, Med. Phys. 39 (4) (2012) 1893–1903.
[24] J.A. MacNeil, S.K. Boyd, Accuracy of high-resolution peripheral quantitative computed tomography for measurement of bone quality, Med. Eng. Phys. 29 (10) (2007) 1096–1105.
[25] P. Varga, E. Dall'Ara, D.H. Pahr, M. Pretterklieber, P.K. Zysset, Validation of an HR-pQCT-based homogenized finite element approach using mechanical testing of ultra-distal radius sections, Biomech. Model. Mechanobiol. 10 (4) (2011) 431–444.
[26] E.M. Lochmuller, N. Krefting, D. Burklein, F. Eckstein, Effect of fixation, soft-tissues, and scan projection on bone mineral measurements with dual energy X-ray absorptiometry (DXA), Calcif. Tissue Int. 38 (3) (2001) 140–145.
[27] Y. Chen, E. Dall Ara, E. Sales, K. Manda, R. Wallace, P. Pankaj, M. Viceconti, Micro-CT based finite element models of cancellous bone predict accurately displacement once the boundary condition is well replicated: a validation study, J. Mech. Behav. Biomed. Mater. 65 (2017) 644–651.
[28] A.I. Birkhold, H. Razi, R. Weinkamer, G.N. Duda, S. Checa, B.M. Willie, Monitoring in vivo (re)modeling: a computational approach using 4D microCT data to quantify bone surface movements, Bone 75 (2015) 210–221.
[29] Y. Lu, M. Boudiffa, E. Dall'Ara, I. Bellantuono, M. Viceconti, Development of a protocol to quantify local bone adaptation over space and time: quantification of reproducibility, J. Biomech. 49 (10) (2016) 2095–2099.
[30] E. Dall'Ara, P. Varga, D. Pahr, P. Zysset, A calibration methodology of QCT BMD for human vertebral body with registered micro-CT images, Med. Phys. 38 (5) (2011) 2602–2608.

[31] A. Laib, P. Rüegsegger, Comparison of structure extraction methods for in vivo trabecular bone measurements, Comput. Med. Imaging Graph. 23 (1999) 69–74.
[32] A. Laib, T. Hildebrand, J. Häuselmann, P. Rüegsegger, Ridge number density: a new parameter for in vivo bone structure analysis, Bone 21 (6) (1997) 541–546.
[33] A. Laib, P. Rüegsegger, Calibration of trabecular bone structure measurements of in vivo three-dimensional peripheral quantitative computed tomography with 28-um-resolution microcomputed tomography, Bone 24 (1) (1999) 35–39.
[34] A.M. Parfitt, M.K. Drezner, F.H. Glorieux, J.A. Kanis, H. Malluche, P.J. Meunier, S.M. Ott, R.R. Recker, Bone histomorphometry: standardization of nomenclature, symbols, and units. Report of the ASBMR histomorphometry nomenclature committee, J. Bone Miner. Res. 2 (6) (1987) 595–610.
[35] T. Hildebrand, P. Rüegsegger, A new method for the model-independent assessment of thickness in three-dimensional images, J. Microsc. 185 (1) (1997) 67–75.
[36] J.M. Bland, D.G. Altman, Statistical methods for assessing agreement between two methods of clinical measurement, Lancet 1 (8476) (1986) 307–310.
[37] G. Maquer, S.N. Musy, J. Wandel, T. Gross, P.K. Zysset, Bone volume fraction and fabric anisotropy are better determinants of trabecular bone stiffness than other morphological variables, J. Bone Miner. Res. 30 (6) (2015) 1000–1008.
[38] K. Sekhon, G.J. Kazakia, A.J. Burghardt, B. Hermannsson, S. Majumdar, Accuracy of volumetric bone mineral density measurement in high-resolution peripheral quantitative computed tomography, Bone 45 (3) (2009) 473–479.
[39] M. Krause, O. Museyko, S. Breer, B. Wulff, C. Duckstein, E. Vettorazzi, C. Glueer, K. Puschel, K. Engelke, M. Amling, Accuracy of trabecular structure by HR-pQCT compared to gold standard muCT in the radius and tibia of patients with osteoporosis and long-term bisphosphonate therapy, Osteoporos. Int. 25 (5) (2014) 1595–1606.
[40] A.J. Burghardt, G.J. Kazakia, S. Majumdar, A local adaptive threshold strategy for high resolution peripheral quantitative computed tomography of trabecular bone, Ann. Biomed. Eng. 35 (10) (2007) 1678–1686.
[41] X.S. Liu, E. Shane, D.J. McMahon, X.E. Guo, Individual trabecula segmentation (ITS)-based morphological analysis of microscale images of human tibial trabecular bone at limited spatial resolution, J. Bone Miner. Res. 26 (9) (2011) 2184–2193.
[42] R. Ellouz, R. Chapurlat, B. Van Rietbergen, P. Christen, J.B. Pialat, S. Boutroy, Challenges in longitudinal measurements with HR-pQCT: evaluation of a 3D registration method to improve bone microarchitecture and strength measurement reproducibility, Bone 63 (2014) 147–157.
[43] J.A. MacNeil, S.K. Boyd, Improved reproducibility of high-resolution peripheral quantitative computed tomography for measurement of bone quality, Med. Eng. Phys. 30 (6) (2008) 792–799.
[44] K. Engelke, B. Stampa, W. Timm, B. Dardzinski, A.E. de Papp, H.K. Genant, T. Fuerst, Short-term in vivo precision of BMD and parameters of trabecular architecture at the distal forearm and tibia, Osteoporos. Int. 23 (8) (2012) 2151–2158.
[45] F. Eckstein, M. Matsuura, V. Kuhn, M. Priemel, R. Muller, T.M. Link, E.M. Lochmuller, Sex differences of human trabecular bone microstructure in aging are site-dependent, J. Bone Miner. Res. 22 (6) (2007) 817–824.
[46] M. Rupprecht, P. Pogoda, M. Mumme, J.M. Rueger, K. Puschel, M. Amling, Bone microarchitecture of the calcaneus and its changes in aging: a histomorphometric analysis of 60 human specimens, J. Orthop. Res. 24 (4) (2006) 664–674.
[47] A.J. Burghardt, J.B. Pialat, G.J. Kazakia, S. Boutroy, K. Engelke, J.M. Patsch, A. Valentinitsch, D. Liu, E. Szabo, C.E. Bogado, M.B. Zanchetta, H.A. McKay, E. Shane, S.K. Boyd, M.L. Bouxsein, R. Chapurlat, S. Khosla, S. Majumdar, Multicenter precision of cortical and trabecular bone quality measures assessed by high-resolution peripheral quantitative computed tomography, J. Bone Miner. Res. 28 (3) (2013) 524–536.
[48] S.L. Manske, Y. Zhu, C. Sandino, S.K. Boyd, Human trabecular bone microarchitecture can be assessed independently of density with second generation HR-pQCT, Bone 79 (2015) 213–221.